Investigation on the thermal gelation of Chitosan/β-Glycerophosphate solutions

M. Abrami[a], C. Siviello[b], G. Grassi[c], D. Larobina[b], M. Grassi[a,*]

[a] Department of Engineering and Architecture, Trieste University, Trieste, Italy
[b] Institute for Polymers, Composites and Biomaterials - National Research Council of Italy, Portici, Naples, Italy
[c] Department of Life Sciences, Cattinara University Hospital, Trieste University, Trieste, Italy

ARTICLE INFO

Keywords:
Chitosan
Thermal gelation
Rheology
Low filed NMR
Mesh size

ABSTRACT

This work deals with the effect of temperature on the thermal-gelation process of water solutions containing chitosan β-glycerolphosphate disodium salt hydrate. In particular, the attention is focused on the role played by temperature on the gel final properties, a very important aspect in the frame of drug delivery systems. The study was performed by combining rheology and low field nuclear magnetic resonance, two approaches that revealed to be highly synergic as they can detect different aspects of the developing polymeric network. This study indicates that 30 °C represent a sort of threshold for both the gelation kinetics and the gel final properties. Indeed, above this temperature, gelation kinetics was rapid and yielded to a strong gel. On the contrary, a slow kinetics and a final weak gel occurred below 30 °C. Finally, rheology and low field NMR allowed, independently, evaluating the time evolution of the network mesh size upon gelation.

1. Introduction

In recent years, controlled drug delivery systems based on hydrogels have been highlighted as therapeutic carriers to deliver different kind of drugs at targeted sites within a specific time frame (Singh & Lee, 2014). Certainly, the possibility of controlling the release rate, the site of action and the drug release duration is relevant as it minimizes possible side effects improving the therapeutic efficacy. Additionally, also the choice of the administration route (oral, ocular, transdermal and subcutaneous, for instance) entails significant consequences. Particularly attracting, because of the general low side effects, is the in situ delivery of drugs (Grassi, Farra, Caliceti, & Grassi, 2005). Most suited for this delivery route are hydrogel-based technologies, which can be easily injected at the site of interest (Li, Toma, & Toma, 2012). The hydrogel is prepared as a gel precursor, which resembles a clear polymer solution easily injectable in-situ. Following injection, in response to changes in external environment, gel-precursor can undergo gelation. Gelation can occur under mild conditions, such as variation in pH, temperature, ionic concentration (Huynh, Nguyen, & Lee, 2011) and/or chemical reactions including Michael addition (Jin et al., 2010), Schiff base (Tan, Chu, Payne, & Marra, 2009) and enzymes addition. Generally, in the frame of environmentally responsive hydrogels, temperature is the easiest stimulus triggering gelation. The advantages of using injectable hydrogels rely on their high moldability (adaptability to every shape), the possibility of in vivo delivery in a minimally invasive way (resulting in a faster recovery, smaller scar size and minimal discomfort for the patient), and the capacity of easily and effectively encapsulating cells and/or drugs. Typically, bioactive molecules or cells can be encapsulated within aqueous polymer solutions (gel precursor) at low temperature, and then turned into a hydrogel, soon after injection into the body due to the rise in temperature rise (Li et al., 2012, Zhou et al., 2015).

In this regard, chitosan-based hydrogels have gained increasing interest as novel and safe delivery systems. Injectable chitosan-based gels have been already employed for drug delivery, tissue bone engineering and cartilages repair (Ruel-Gariépy et al., 2004). Chitosan (CS), structurally similar to glycosaminoglycans, and produced by deacetylation of the glucose derivative chitin, is comprised of glucosamine ($G1cNH_2$) and acetyl-glucosamine (G1cNAc) units. CS has excellent biocompatibility, low toxicity and immunostimulatory activities (Souza, Zahedi, Allen, & Piquette-Miller, 2009).

However, CS is soluble only in aqueous acid media (at pH ≤ 6.5) since under this condition its free amino groups are protonated thus conferring to the molecule a positive charge. As this condition does not reflect the physiological pH, the use of chitosan alone is not ideal. To overcome this limitation, it is possible to neutralize the positive charges by the addition of the salt β-glycerolphosphate (β-GP). β-GP allows the maintenance of chitosan in a soluble form in condition of pH near the

* Corresponding author at: Department of Engineering and Architecture, University of Trieste, Via Valerio 6, Trieste, I-34127, Italy.
E-mail address: mario.grassi@dia.units.it (M. Grassi).

Accepted 4 March 2019

neutral, resembling the physiological pH. Additionally, β-GP also allows the sol-gel transition upon heating. Probably, heating induces proton transfer from chitosan to β-GP, thereby neutralizing CS and allowing attractive inter-chain forces to form a physical gel (Cho, Heuzey, Begin, & Carreau, 2006). Due to the above features, CS/β-GP represents a very intriguing thermo-sensitive hydrogel. The literature on CS/β-GP is quite broad and it substantially diversifies into two branches: the first focused on understanding the mechanisms of sol-gel transition (Filion, Lavertu, & Buschmann, 2007), the second, regardless of the underlying mechanism, analyses the effect of the initial variables (Dalmoro et al., 2017) on the gelation temperature. Our work is, instead, focused on a less discussed topic, i.e., the effect of temperature on the system final structural properties. Depending on the final application of the CS/β-GP system, the considered temperature can be different and, consequently, also gel mechanical characteristics can differ. The combined use of low field nuclear magnetic resonance (LF-NMR) and rheology offers an innovative approach for studying the thermo-gelation process.

2. Materials and methods

CS (viscosity 428 cPs, CAS n. 9012-76-4), β-GP disodium salt hydrate (β-GP) (≤1.0 mol % L-α-isomer, ≤0.1% inorganic phosphorus, molecular weight 216.04, CAS n. 154804-51-0) and acetic acid (AcOH, CAS n. 64-19-7) were purchased from Sigma-Aldrich s.r.l. (Milan, Italy) and used without further purification.

The fraction of acetylated units of CS was determined by ^{1}H NMR (Sacco, Cok, Asaro, Paoletti, & Donati, 2018). Prior to the analysis, the chitosan sample was slightly depolymerized to increase the resolution of the spectrum (Tømmeraas, Vårum, Christensen, & Smirsrød, 2001). CS samples were prepared as it follows: 20 mg of polymer were solubilized in 2 mL of D_2O + 150 μL of DCl 1 M under vigorous stirring. Then, 30 μL of $NaNO_2$ 10 mg/mL in D_2O were added and the solution stirred for 2 h. Finally, 700 μL of CS sample were transferred into NMR tubes and analyzed at 85 °C by means of a Varian VNMRS NMR spectrometer (11.74 T) operating at 499.65 MHz for proton. The chemical shifts are expressed in ppm downfield from the signal for 3-(trimethylsilyl)propanesulfonate. The ^{1}H NMR spectrum of chitosan is reported in Fig. 1S of the supporting information. Indicating A_{Ac} as the area of the protons of the methyl group of GlcNAc units (approx. at 2.05 ppm) and A_{NH2} as the area of the proton at the C2 of the $GlcNH_2$ units (approx. at 4.9 ppm), the residual degree of acetylation (DA) can be calculated as:

$$DA(\%) = \frac{\frac{1}{3}A_{AC}}{A_{NH2} + \frac{1}{3}A_{AC}} \cdot 100 \quad (1)$$

The degree of deacetylation (DDA) is, then, calculated as:

$$DDA(\%) = 100 - DA(\%) \quad (2)$$

The residual degree of acetylation (DA(%)) of this CS resulted to be 22% so that the deacetylated fraction (DDA(%)) was 78%.

The CS viscosity average molecular weight (M_w) was evaluated to be 213 kDa from intrinsic viscosity measurements, in agreement with the producer specification (190–310 kDa). Indeed, the intrinsic viscosity of chitosan, in a 1% acetic acid solution, was measured being around 32.5 ml/g. The application of Mark-Houwink equation with $K = 4.74\ 10^{-3}$ ml/g, $a = 0.72$ (Kasaai, 2007) gave the above reported value of M_w.

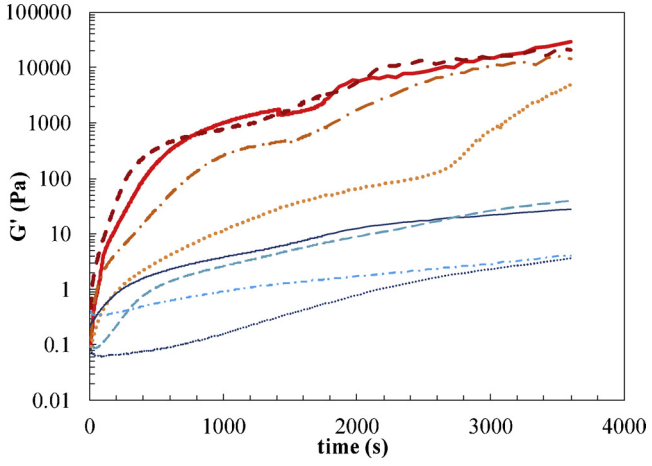

Fig. 1. Time Sweep test. Evolution of *G*' in CS/β-GP system at different temperatures 15 °C (dashed/dotted light blue line), 20 °C (dotted blue line), 25 °C (dashed light blue line), 27 °C (solid blue line), 30 °C (dotted orange line), 37 °C (dashed/dotted orange line), 45 °C (dashed dark red line) and 47 °C (solid red line) (1 Hz, 1 Pa). CS = 0.087 M, βGP/CS molar ratio = 2.11, AcOH/CS molar ratio = 0.6 (For interpretation of the references to colour in this figure legend, the reader is referred to the web version of this article).

2.1. Preparation of thermo-sensitive chitosan hydrogel

For the realization of thermo-sensitive hydrogels, CS and β-GP aqueous solutions were separately prepared and then mixed together, based on a protocol we previous developed (DalMoro et al., 2017). While chitosan concentration and βGP/CS molar ratio were set, respectively to 0.087 M and 2.11, two different AcOH/CS molar ratios were considered (0.6 and 0.48).

For the LF-NMR and rheological characterization, CS solution was prepared dissolving 2 g of polymer in 100 ml of an AcOH solution at 0.60 or 0.48 M ratio AcOH/CS. The solution, mixed overnight at room temperature, was, then, filtered under vacuum. Due to CS lost during filtration, the actual CS weight percentage was determined by weighing a portion of the filtered solution before and after drying. β-GP solution was prepared by dissolving a known amount of β-GP into a known volume of water so that: i) the final β-GP/CS mole ratio was equal to 2.11; ii) the final molar concentration of CS monomer was equal to 0.087 M (about 1.5%w/w). The β-GP solution was, then, added drop wise to the CS solution under rapid stirring, maintaining the temperature at 4 °C. The final solution was stored at 4 °C for 24 h before testing.

2.2. Rheology

Rheological measurements were performed by a stress controlled rotational rheometer (Haake Mars Rheometer, 379-0200 Thermo Electron GmbH, Karlsruhe, Germany) equipped by parallel plate geometry (PP35, φ = 35 mm, serrated surfaces to avoid slippage at the wall) with a gap of 0.8 mm. The measuring device was kept inside a glass bell at saturated humidity conditions to avoid evaporation effects. In order to study the gelation kinetics, time-sweep tests (1 Hz and 1 Pa) were performed in isothermal conditions at several temperatures, (15, 20, 25, 27, 30, 37, 45 and 47 °C). After gelation, the CS-βGP systems were characterized by means of stress sweep tests (1 Hz) to assess the wideness of the linear viscoelastic region. Then, frequency sweep tests, performed inside the linear viscoelastic region (τ = 1 Pa), allowed the determination of systems mechanical spectra (elastic (*G*') and viscous (*G*'') moduli dependence on the solicitation frequency *f*).

The evaluation of the average network mesh size (ξ_{RHEO}) was performed assuming that the shear modulus of the gels (*G*) is represented by the average *G*' value over the frequency range explored and that Flory theory holds (Flory, 1953):

$$\rho_x = G/RT \quad (3)$$

where ρ_x is the network crosslink density ρ_x (defined as the moles of junctions between different polymeric chains per hydrogel unit volume), *T* is temperature and *R* is the universal gas constant. The link between ρ_x and ξ_{RHEO} is provided by the equivalent network theory (Schurz, 1991), according to which the following relation holds:

$$\xi = \sqrt[3]{6/\pi\rho_x N_A} \quad (4)$$

where N_A is Avogadro number.

2.3. LF-NMR

LF-NMR characterization was performed at different temperatures (15, 20, 25, 27, 30, 37, 45 and 47 °C) by means of a Bruker Minispec mq20 (0.47 T, Germany). The determination of the average water protons transverse (spin-spin) relaxation time (T_{2m}) was performed according to the CPMG sequence (Carr–Purcell–Meiboom–Gill) (Meiboom & Gill, 1958) {90°[-τ-180°-τ(echo)]$_n$-T_R} with a 8.36 μs wide 90°pulse, τ = 250 μs, and T_R (sequences repetition rate) equal to 5 s. As our samples were characterized by very different T_{2m} values ranging from about 200 ms up to 1200 ms, *n* was not the same for all samples. The criterion adopted to choose *n* consisted in ensuring that the final FID intensity were about 2% of the initial FID intensity (in the light of this acquisition strategy, we verified that it was un-necessary adopting $T_R > 5$ s). Finally, each FID decay, composed by *n* points, was repeated 36 times (number of scans). The relaxation times distribution (A_i, T_{2i}) was determined by fitting the FID time decay (*Is*), related to the extinction of the *x*–*y* component of the magnetization vector (M_{xy}), according to its theoretical estimation *I*(t) (Chui, Phillips, & McCarthy, 1995):

$$I(t) = \sum_{i=1}^{m} A_i exp(-t/T_{2i}) \quad T_{2m} = \sum_{i=1}^{m} A_i T_{2i} / \sum_{i=1}^{m} A_i \quad (5)$$

where *t* is time, A_i are the pre-exponential factors (dimensionless) proportional to the number of protons relaxing with the relaxation time T_{2i} and T_{2m} is the average relaxation time of protons. For its more immediate meaning, the % value of A_i was reported ($A_{i\%}$) in place of A_i value:

$$A_{i\%} = 100 * A_i / \sum_{i=1}^{m} A_i \quad (6)$$

The number, *m*, of the relaxation times (T_{2i}) constituting the relaxation time distribution (A_i, T_{2i}) was determined by minimizing the product $\chi^{2*}(2m)$, where χ^2 is the sum of the squared errors and 2*m* represents the number of fitting parameters of Eq.(5) (Draper & Smith, 1966).

The determination of the average mesh size ($\xi_{LF\text{-}NMR}$) of CS-βGP gels was performed according to a recently proposed (Abrami et al., 2018) simplified equation describing the relaxation of water hydrogens entrapped in a "solid" structure such as a three-dimensional polymeric network (Brownstein & Tarr, 1979; Chui et al., 1995; Scherer, 1994):

$$\left(\frac{1}{T_2}\right)_m = \frac{1}{T_{2H2O}} + \frac{S}{V}\mathcal{M} = \frac{1}{T_{2H2O}} + 2\frac{\mathcal{M}}{R_f \frac{1-0.58\varphi}{\varphi}} \quad (7)$$

$$\xi_{LF\text{-}NMR} = R_f \sqrt{\frac{1-0.58\varphi}{\varphi}} \quad (8)$$

where $(1/T_2)_m$ is the average value of $1/T_2$, T_{2H2O} is the relaxation time of bulk water hydrogens (i.e. water far from polymeric chains), *S* is the polymeric chains surface, *V* is water volume, φ is the polymer volume fraction and monotype corsiva is a parameter, called relaxivity, representing the ratio between the thickness and the relaxation time of the water layer adhering to the polymeric chains surface (bound water).

3. Results and discussion

The chitosan used in the present study was characterized, as to the residual degree of acetylation, DA(%), by means of ^{1}H-NMR measurements. Several methods have been proposed for the determination of DA(%) for chitosan: IR, UV, gel permeation chromatography, colloid titration, elemental analysis, dye adsorption, and acid-base titration methods (Roberts, 1992). These methods have been reported to be only partially quantitative and relatively cumbersome (Einbu & Vårum, 2004). Proton NMR spectroscopy is a convenient and accurate method for determining the chemical composition of chitosan (Hirano & Yamaguchi, 1976; Kasaai, 2010; Vårum, Antohonsen, Grasdalen, & Smidsrød, 1991). As reported in the Material and Methods section, the residual degree of acetylation, DA(%), was found to be 22%.

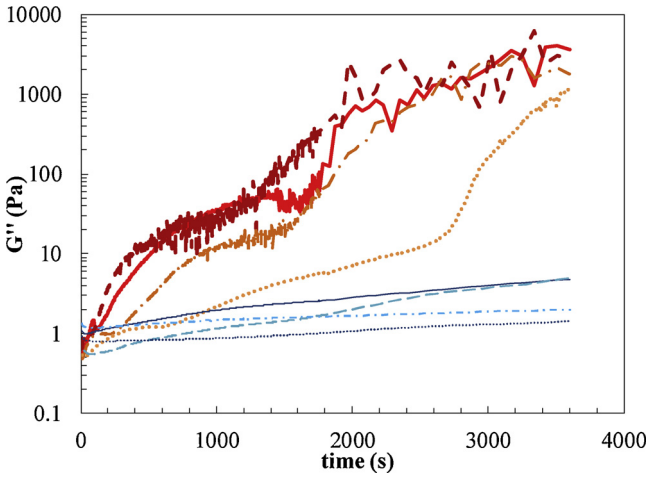

Fig. 2. Time Sweep test. Evolution of *G*" in CS/β-GP system at different temperatures 15 °C (dashed/dotted light blue line), 20 °C (dotted blue line), 25 °C (dashed light blue line), 27 °C (solid blue line), 30 °C (dotted orange line), 37 °C (dashed/dotted orange line), 45 °C (dashed dark red line) and 47 °C (solid red line) (1 Hz, 1 Pa). CS = 0.087 M, βGP/CS molar ratio = 2.11, AcOH/CS molar ratio = 0.6 (For interpretation of the references to colour in this figure legend, the reader is referred to the web version of this article).

The sol-gel transition related to the CS/β-GP system was monitored under isothermal conditions by evaluating the time evolution of rheological properties and the average relaxation time of water protons (LF-NMR). Figs. 1 and 2 show, respectively, the time evolution of the storage (*G*') and the loss (*G*") moduli at different temperatures (20, 25, 27, 30, 37, 45 and 47 °C). Figs. 1 and 2 indicate that the *G*' and *G*" time evolutions can be roughly grouped into two classes depending on temperature. Indeed, for $T \geq 30$ °C, the final values of both *G*' and *G*" competing to different temperatures (30, 35, 40 and 47 °C) are not so different each other and they detach from those competing to lower temperatures (15, 20, 25 and 27 °C) that, in turn, are similar among them. For $T \geq 30$ °C, an "early" gelation (gel point < 180 s) followed by a "fast" increase of *G*' and *G*" takes place, while just few degree below 30 °C, a "slow" monotonic increase and a "late" gel-point time (≥ 270 s) occurs (Figs. 1 and 2).

For different temperatures, the crossover between *G*' and *G*" occurs, respectively, at: $T = 15$ °C, 1970s; $T = 20$ °C, 499 s; $T = 25$ °C, 399 s; $T = 27$ °C, 270 s; $T = 30$ °C, 175 s; $T = 37$ °C, 45 s; $T = 45$ °C, 14 s; $T = 47$ °C, 10 s. These evidences let us concluding that temperature not only drives the gelation process but it also affects the final gel rheological properties in a discontinuous manner (i.e. below or over 30 °C). Indeed, the gelation pattern shown in Figs. 1 and 2 reveals that the monotonic increase of *G*' and *G*" proceeds by a slowly decreasing slope for $T < 30$ °C. On the contrary, it displays an abrupt increase, after about 1200s, for $T \geq 30$ °C. The behavior at "lower" temperatures can be reasonably connected to a progressive reduction of CS segments mobility, while that at "higher" *T* could be, in principle, due to either an increase in CS segments mobility, or a change in the driving force of the gelling process. We conjecture that an increase in the driving force of gelation, i.e. in the interaction between CS segments, is the reason for slope increase (acceleration of gelation). To support this idea, we recall that the sol-gel transition occurring in an acidified solution of CS containing β-GP is described (Filion et al., 2007; Lavertu, Filion, & Buschmann, 2008) as the consequence of a phase separation induced by

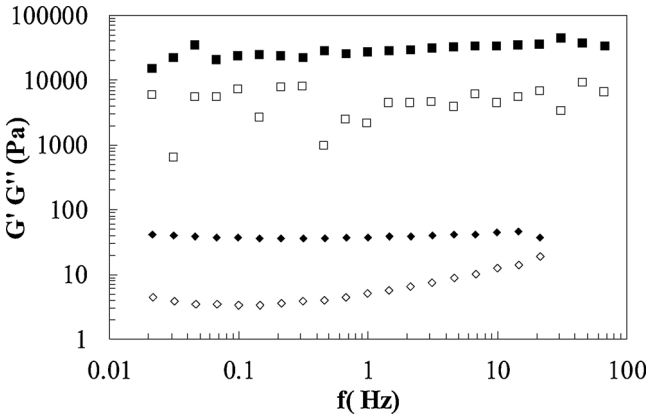

Fig. 3. Mechanical spectra referring to CS/β-GP system at 25 °C (*G*' ♦, *G*" ◊) and 47 °C (*G*' ■, *G*"□) (τ = 1 Pa). CS = 0.087 M, βGP/CS molar ratio = 2.11, AcOH/CS molar ratio = 0.6.

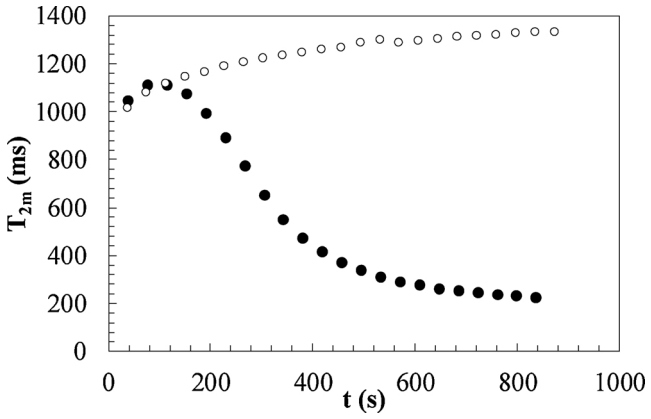

Fig. 4. Time evolution of the average relaxation time (T_{2m}) referring to a water solution containing chitosan and the crosslinking agent (βGP) (closed circles), and an identical solution containing only chitosan (open circles). CS = 0.087 M, βGP/CS molar ratio = 2.11, AcOH/CS molar ratio = 0.6. Heating temperature is 37 °C.

a proton transfer from CS to β-GP. Actually, an increase in temperature is responsible of such transfer that depresses poly-cations repulsion and that raises hydrophobic and hydrogen bonding inter-chain forces, allowing system crosslinking. In this light, we speculated that a further proton transfer from CS to β-GP occurs in the late stage of phase separation for $T \geq 30$ °C, thus affecting the final gelation process. Indeed, as phase separation proceeds, the local concentration of CS monomers increases up to provoke a further proton transfer (from CS to β-GP). Consequently, additional physical interactions can occur and the crosslinking process experiences an acceleration. Potentiometric titrations performed on CS solutions partially support the above hypothesis (Filion et al., 2007). Indeed, by continuously adding a strong base (NaOH 1 M) to an acidified solution of CS (without β-GP), Filion and co-authors (Filion et al., 2007) observed an initial increase of pH followed, after gelation, by a pH reduction, despite the increase in NaOH concentration.

Frequency-sweep tests, performed at the end of each time sweep experiment, confirmed the gel nature of all the studied systems, regardless of the gelation temperature (Fig. 3). For the sake of clarity, Fig. 3 shows the mechanical spectra referring to the gels obtained at 47 °C and 25 °C, being these systems representative of the two groups (i.e. those gelled at $T < 30$° and those gelled at $T \geq 30$ °C). It can be seen that, in both cases (T = 47 °C and 25 °C), *G*' is > > *G*" and both moduli are, substantially, frequency independent. The fact that *G*' and *G*" values competing to 47 °C are about three orders of magnitude bigger than those referring to 25 °C clearly demonstrates that temperature affects also the final gel properties and not only the time evolution of the gelation process.

Low field NMR can be profitably employed to study the variation of the spatial organization of CS polymeric chains upon gelation by following the effect of gel structure formation on the average relaxation time (T_{2m}) of protons belonging to water molecules. Indeed, T_{2m} depends on many factors such as temperature, magnetic field intensity, and the interaction of hydrogens with other possible substances (solid components) present in the environment (Gallegos, Munn, Smith, & Stermer, 1987). When the magnetic field is 0.47 T, the relaxation time of pure water hydrogens at 25 °C is $T_{2H2O} \approx 3000$ ms while it increases up to about 3700 ms at 37 °C (Coviello et al., 2013). The effects of solubilized/dispersed substances (such as the CS/β-GP polymeric chains) on T_{2m} is due to the fact that the relaxation time of water protons magnetization near the solid surface (bound water) is lower (fast relaxation) than that (slow relaxation) of bulk water protons (free water) that are unaffected by solid surface (Chui et al., 1995). Accordingly, the average relaxation time of protons (T_{2m}) will depend on the ratio between the solid surface (*S*, proportional to the number of protons close to *S*) and the water volume (*V*, proportional to the total number of hydrogens belonging to the system) (Brownstein & Tarr, 1979). Consequently, it turns out that T_{2m} is connected to the ratio *S*/*V* via an inverse proportionality relation (Abrami et al., 2018; Gallegos et al., 1987). As the gelation process of CS/β-GP entails phase separation, it seems reasonable that it reflects in a variation of *S*/*V*, which, in turn, implies a T_{2m} variation. Thus, as the CS/β-GP gelation is induced by a temperature increase, T_{2m} time variation will be the results of two phenomena, i.e. temperature increase and gel network formation. In order to enucleate the effect of both phenomena, Fig. 4 shows the T_{2m} time evolution referring to two solutions heated from 10 °C to 37 °C.

While the first one cannot give origin to a gel network upon temperature increase, as it contains only CS (open circles), the second one can form a gel, as it contains both CS and the crosslinking agent β-GP (closed circles). It is clear that when the crosslinking reaction does not occur (open symbols), T_{2m} monotonically increases due to solution heating from 10 °C to 37 °C. On the contrary, when β-GP is present, crosslinking can occur and both phenomena (temperature increase and gel network formation) affect the T_{2m} time variation. Fig. 4 shows that after an initial increase, due to temperature rise, T_{2m} decreases, due to gel network formation, up to the attainment of a gel condition. This means that, in the beginning, the temperature effect prevails on the gel network formation while, then, gel network formation plays the role of predominant phenomenon in ruling T_{2m} time evolution. Provided to be in the temperature range 30–47 °C, the above described behavior is similar regardless the temperature as witnessed by Fig. 5. On the contrary, when the heating temperature is below 30 °C, the presence of the maximum in the T_{2m} vs *t* trend is much less evident and curve shape modifies with temperature (see Fig. 6). The similarity of the T_{2m} vs *t* curves for $T \geq 30$° is supported by the possibility of collapsing them on a master curve (see Fig. 7) by a simple shift on the time axis according to a shift factor τ.

Once again, the proton transfer mechanism from CS poly-cation to β-GP (Lavertu et al., 2008) rules the observed behavior. At the heating temperature (T_H), the ionic equilibrium between the two charged molecules, usually quantified as the degree of ionization of the poly-cation (α), changes as well. As Lavertu and co-worker described (Lavertu et al., 2008), when T_H reaches the precipitation temperature T_p (phase separation) it is possible to observe that α reaches the precipitation value α_p. Further increase in temperature ($T > T_p$) have only minor effect on the value of α_p. At α_p, the gelation starts. The presence of a master-curve confirms that once the maximum degree of ionization (α_p) is reached, there is no further effect of α on the gelation kinetics, which, at this point, is only dominated by diffusive phenomena. A further increase in T_H ($> T_p$) simply results in an acceleration of the gelation process. On

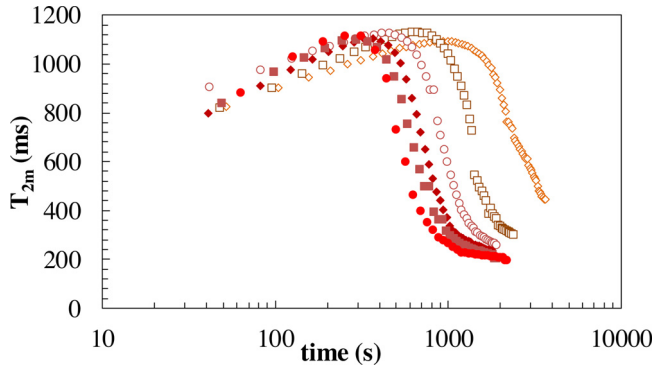

Fig. 5. Time evolution of the relaxation time, T_{2m}, for CS/β-GP systems at different heating temperature: 30 °C (orange empty diamonds), 35 °C (brown empty squares), 37 °C (red empty circles), 40 °C (red filled diamonds), 45 (brown filled squares), 47 °C (red filled circles). CS = 0.087 M, βGP/CS molar ratio = 2.11, AcOH/CS molar ratio = 0.6 (For interpretation of the references to colour in this figure legend, the reader is referred to the web version of this article).

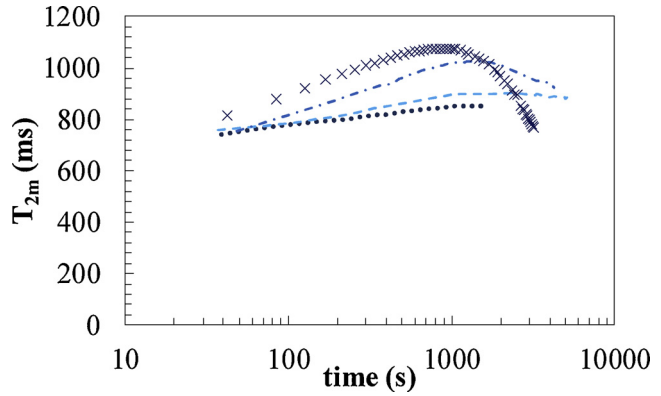

Fig. 6. Time evolution of relaxation time, T_{2m}, for CS/β-GP systems at different heating temperature: 15 °C (blue dots), 20 °C (dashed light blue line), 25 °C (dashed/doted blue line), 27 °C (blue crosses). CS = 0.087 M, βGP/CS molar ratio = 2.11, AcOH/CS molar ratio = 0.6 (For interpretation of the references to colour in this figure legend, the reader is referred to the web version of this article).

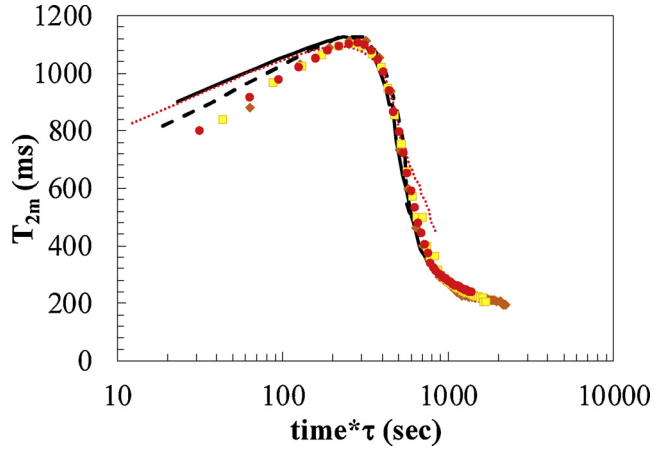

Fig. 7. T_{2m} master curve for CS-βGP system at different temperatures: 30 °C (red small dots), 35 °C (dashed black line), 37 (solid black line), 40 °C (red big dots), 45 °C (yellow squares), 47 °C (orange diamonds). τ is the shifting factor. CS = 0.087 M, βGP/CS molar ratio = 2.11, AcOH/CS molar ratio = 0.6 (For interpretation of the references to colour in this figure legend, the reader is referred to the web version of this article).

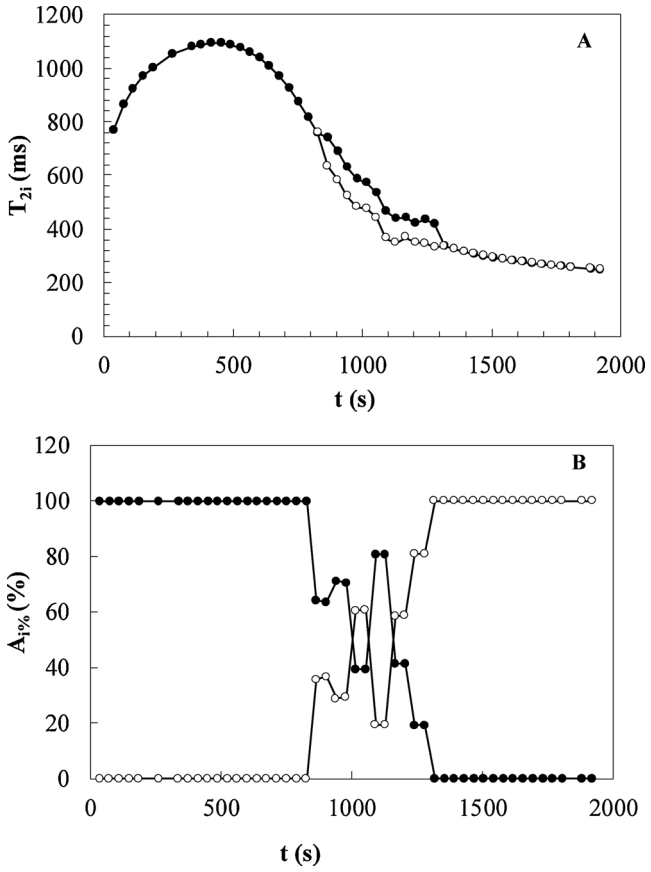

Fig. 8. (A) Time evolution of the two relaxation times (T_{21} •; T_{22} ○) when heating temperature is 37 °C. (B) Temporal evolution of the relative abundance (A_1•; A_2 ○) of the two relaxation times T_{21}, T_{22} shown in A. CS = 0.087 M, βGP/CS molar ratio = 2.11, AcOH/CS molar ratio = 0.6.

the contrary, for $T_H < T_p$ the degree of ionization has not yet reached its precipitation value α_p. Nevertheless, CS still has the tendency to irreversibly aggregate with the concomitant occurrence of a gel. However, in these cases, we speculate that the dynamic rearrangements of the charges on the poly-cations regulate the mechanism by which the now "slow" precipitation occurs. Indeed, for $T < 30°C$ a systematic reduction of the T_{2m} slope as well as of the rheological curves occurs.

Based on the data of Fig. 5 and 7, it turns out that τ depends on temperature according to a power law ($\tau = 2.51*105*T^{3.25}$; $r^2 = 0.958$).

The threshold role played by $T = 30$ °C is also proved by the fact that for $T < 30$ °C, T_{2m} is characterized by only one relaxation time ($T_{2m} = T_{21}$) in its entire time evolution, whereas for $T \geq 30$ °C, two relaxation times (T_{21} and T_{22}) appear in the middle part of T_{2m} evolution (Fig. 8A, heating temperature 37 °C). It can be argued that the gelling process implies the temporary formation of two pseudo-phases, one richer in polymer and the other poorer in polymer. More precisely, it could be supposed that the different relaxation times depend on local polymeric concentration. Accordingly, the richer polymer phase is characterized by a lower relaxation time (T_{22}), while the poorer polymer phase is characterized by a higher relaxation time (T_{21}). Upon gelation, the amplitude related to the polymer reach phase (A_{22}, T_{22}) prevails on detriment of the poor one (A_{21}, T_{21}), which, finally, disappears (Fig. 8B). Similar results occur for all experiments performed at $T \geq 30$ °C.

All the above considerations allow concluding that, similarly to the rheological tests, also LF-NMR characterization seems to subdivide the systems in two categories: below and above a heating temperature of 30 °C.

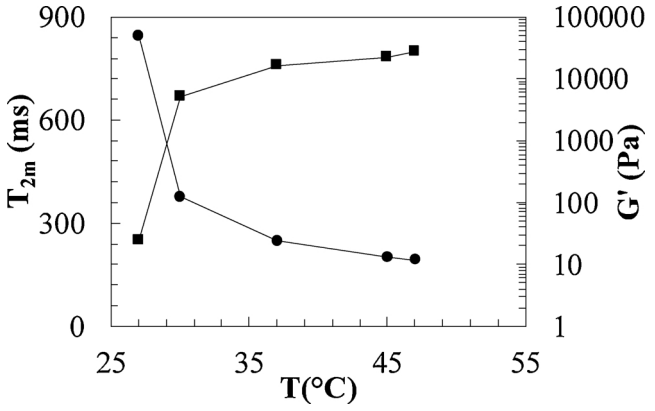

Fig. 9. Elastic modulus G'(1 Hz) (black squares) and average relaxation time T_{2m} (black circles) referring to CS-βGP system at the end of the isothermal test performed at different temperatures: 15, 20, 25, 27, 30, 35, 37, 45, 47 °C.

In order to merge the information coming from the LF-NMR and the rheological characterization, Fig. 9 shows the effect of heating temperature on G' (evaluated at 1 Hz) and T_{2m} measured when the gelation process has been completed (i.e., at the end of the isothermal test). The inverse behavior of G' and T_{2m} with increasing temperature is due to the same reason, i.e. the formation of a more and more articulated/interconnected polymeric network that reflects in a stiffer structure characterized by an increased S/V ratio. As the abrupt variation of both G' and T_{2m} occurs at the same temperature ($T \approx 27$ °C), it turns out, again, the threshold role played by $T = 30$ °C for the gelation process. In addition, the inverse proportionality between G' and T_{2m} (see Fig. 9) agrees with what theoretically predicted in the case of gels (Fanesi et al., 2018) when dangling chains do not exist in the network or their fraction is negligible (Chiarappa et al., 2017).

As the results obtained for AcOH/CS = 0.6 are very similar when AcOH/CS = 0.48 (data not shown), we can conclude that, in this range, the effect of the AcOH/CS ratio on gel architecture/properties is negligible.

We conclude the characterization of our system (CS/β-GP, AcOH/CS = 0.6) by focusing on the estimation of gel mesh size resorting to rheology and LF-NMR. In particular, we would like to evaluate how the crosslinking reaction affects the mesh size of the forming three-dimensional polymeric network. As qualitatively similar results were obtained for $T \geq 30°$, the attention was focussed on the intermediate temperature value of $T = 37$ °C. The main assumption is that the average value of the elastic modulus (G') essentially represents the shear modulus (G) of the forming gel. Obviously, this is substantially true only when G' is much higher (about ten times) than the loss modulus G'', this taking place after about 500 s (see Fig. 1 and 2) for $T = 37$ °C. Thus, Eqs. (3) and (2) allow the estimation of the time evolution of the gel mesh size (ξ_{RHEO}) as shown in Fig. 10.

In the case of the LF-NMR approach, we assume that a real gel network occurs only after the maximum exhibited by the time variation of the average relaxation time (T_{2m}) as shown, for example, in Fig. 5. Indeed, as above discussed, before the maximum, the variation of T_{2m} is mainly due to system heating and only, then, the effect of the developing three-dimensional network becomes relevant on T_{2m}. For $T = 37$ °C, this condition takes place after about 500 s since the beginning of the crosslinking reaction (see Fig. 5). The strategy adopted to evaluate the mesh size evolution according to LF-NMR ($\xi_{LF\text{-}NMR}$) relies on Eqs. (7) and (8). Assuming that monotype corsiva does not depend on the crosslinking degree (a typical assumption in the LF-NMR frame), Eq. (8) allows monotype corsiva evaluation when the gel is completely formed. This condition, for $T = 37$ °C, occurs after about 32 min when $(1/T_2)_m = 4*10^{-3}$ s^{-1} (Fig. 5). Knowing that $R_f \approx 1$ nm (monomer size have been estimated by structural data (Mazeau, Winter, & Chanzy, 1994)), T_{2H2O} (37 °C) = 3.694 s (Coviello et al., 2013) and

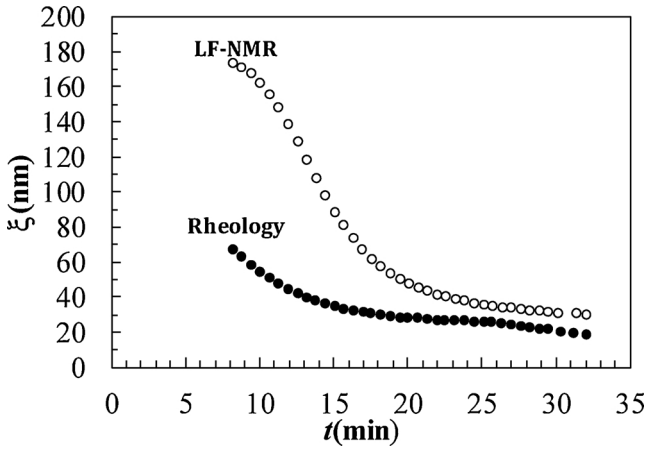

Fig. 10. Time evolution (t) of the gel mesh size (ξ) according to the rheological (•) and the LF-NMR approaches (○). Data refer to the heating temperature of 37 °C. CS = 0.087 M, βGP/CS molar ratio = 2.11, AcOH/CS molar ratio = 0.6.

$\varphi = 1.04*10^{-2}$, Eq. (7) yields to monotype corsiva = $1.79*10^{-7}$ m/s. Interestingly, this monotype corsiva value resembles what found in low concentration scleroglucan–borax and guar gum–borax hydrogels (0.7% w/v) (Coviello et al., 2013). Relaying on monotype corsiva knowledge, it is possible establishing a connection between the mesh size of the developing network and its relaxation time (the experimental datum) by a simple mathematical manipulation of Eqs. (7) and (8):

$$\xi = 2\mathscr{M}\sqrt{\frac{1\text{-}0.58\varphi}{\varphi}} \Big/ \left(\left(\frac{1}{T_2}\right)_m - \frac{1}{T_{2H2O}}\right) \quad (9)$$

Eq. (9) shape (white circles) is depicted in Fig. 10 and it is compared with the outcomes deriving from the rheological approach (black circles). It can be seen that the two approaches converge to very similar results only when the gel is almost completely developed. This is not surprisingly in the light of the different heating kinetics of the sample. Indeed, while both in the rheological and LF-NMR characterisation sample volume is approximately the same (≈ 1 cm^3), the "rheological" heating surface is about 2 times that of the LF-NMR. In addition, while in the rheological case the sample is in direct contact with the heating surface (the inferior sensor plate), in the LF-NMR situation, a glass wall, constituting the sample holder and 0.5 mm thick, separates the sample from the heating source. Thus, it seems reasonable that the faster rheological heating reflects on a more rapid gelation kinetics with respect to the LF-NMR case.

4. Conclusions

In conclusion, the combination of rheology and LF-NMR allowed the description of the gelation kinetics of CS/β-GP systems in response to different heating temperatures. The use of these two macroscopic techniques permitted the evaluation of the system macro and nano-variation occurring upon thermal gelation. In particular, rheology was devoted to evaluate the time evolution of system viscoelastic properties, while rheology and LF-NMR allowed the estimation of the time evolution of the polymeric network mesh size. Interestingly, both approaches lead to similar estimation of the average polymeric mesh size. All these aspects could be very important in the light of final applications that imply an in situ gel formation. Indeed, although the G'-G'' crossover takes place at every temperature (among those considered), when $T < 30$ °C, the gel final properties could be too weak to guarantee the minimal gel residence time at the site of action. However, for $T < 30$ °C, the system guarantees an easy injection because its rheological properties are closer to that of a liquid than to that of a solid material. Thus, this study suggests that the proposed formulation should be prepared at low temperature, injected at the site of action (maintaining $T < 30$ °C)

where the physiological temperature induces the formation of a strong gel able to perform its effect, for example, by releasing a drug. In this sense, the knowledge of the polymeric network mesh-size could play a very important role in system optimization in relation of drug dimension.

Acknowledgements

This research did not receive any specific grant from funding agencies in the public, commercial, or not-for-profit sectors. The authors would like to thank a lot prof. Ivan Donati for the determination of CS de-acetylation fraction.

Appendix A. Supplementary data

Supplementary material related to this article can be found, in the online version, at doi:https://doi.org/10.1016/j.carbpol.2019.03.015.

References

Abrami, M., Chiarappa, G., Farra, R., Grassi, G., Marizza, P., & Grassi, M. (2018). Use of low field NMR for the characterization of gels and biological tissues. *ADMET & DMPK, 6*(1), 34–46.

Brownstein, K. R., & Tarr, C. E. (1979). Importance of classical diffusion in NMR studies of water in biological cells. *Physical Review A, 19*, 2446–2453.

Chiarappa, G., Abrami, M., Dapas, B., Farra, R., Trebez, F., Musiani, F., et al. (2017). Mathematical modeling of drug release from natural polysaccharides based matrices. *Natural Product Communications, 12*, 873–880.

Cho, J., Heuzey, M. C., Begin, A., & Carreau, P. J. (2006). Chitosan and glycerophosphate concentration dependence of solution behaviour and gel point using small amplitude oscillatory rheometry. *Food Hydrocolloids, 20*, 936–945.

Chui, M. M., Phillips, R. J., & McCarthy, M. J. (1995). Measurement of the porous microstructure of hydrogels by nuclear magnetic resonance. *Journal of Colloid and Interface Science, 174*, 336–344.

Coviello, T., Matricardi, P., Alhaique, F., Farra, R., Tesei, G., Fiorentino, S., et al. (2013). Guar gum/borax hydrogel: Rheological, low field NMR and release characterizations. *Express Polymer Letters, 7*, 733–746.

Dalmoro, A., Abrami, M., Galzerano, B., Bochicchio, S., Barba, A. A., Grassi, M., et al. (2017). Injectable chitosan/β-glycerophosphate system for sustained release: gelation study, structural investigation, and erosion tests. *Current Drug Delivery, 14*, 216–223.

Draper, N. R., & Smith, H. (1966). *Applied regression analysis.* New York: John Wiley & Sons.

Einbu, A., & Vårum, K. M. (2004). Structure-property relationships in chitosan. In P. Tomasik (Ed.). *Chemical and Functional Properties of food Saccharides* (pp. 217–230). CRC Press.

Fanesi, G., Abrami, M., Zecchin, F., Giassi, M., Dal Ferro, E., Boisen, A., et al. (2018). Combined used of Rheoloy and LF-NMR for the characterization of PVP-Alginates gels containing liposomes. *Pharmaceutical Research, 35*(171), 1–11.

Filion, D., Lavertu, M., & Buschmann, M. D. (2007). Ionization and solubility of chitosan solutions related to thermosensitive chitosan/glycerol-phosphate systems. *Biomacromolecules, 8*, 3224–3234.

Flory, P. J. (1953). *Principles of polymer chemistry.* Cornell University Press.

Gallegos, D. P., Munn, K., Smith, D. M., & Stermer, D. L. (1987). A NMR technique for the analysis of pore structure: Application to materials with wee-defined pore structure. *Journal of Colloid and Interface Science, 119*, 127–140.

Grassi, G., Farra, R., Caliceti, P., & Grassi, M. (2005). Temperature-sensitive hydrogels: Potential therapeutic applications. *American Journal of Drug Delivery, 3*, 239–251.

Hirano, S., & Yamaguchi, R. (1976). N-Acetylchitosan gel: A polyhydrate of chitin. *Biopolymers, 15*, 1685–1691.

Huynh, C. T., Nguyen, M. K., & Lee, D. S. (2011). Injectable block copolymer hydrogels: Achievements and future challenges for biomedical applications. *Macromolecules, 44*, 6629–6636.

Jin, R., Teixeira, L. S. M., Krouwels, A., Dijkstra, P. J., van Blitterswijk, C. A., Karperien, M., et al. (2010). Synthesis and characterization of hyaluronic acid-poly(ethylene glycol) hydrogels via Michael addition: An injectable biomaterial for cartilage repair. *Acta Biomaterialia Odontologica Scandinavica, 6*, 1968–1977.

Kasaai, M. (2007). Calculation of Mark–Houwink–Sakurada (MHS) equation viscometric constants for chitosan in any solvent–temperature system using experimental reported viscometric constants data. *Carbohydrate Polymers, 68*, 477–488.

Kasaai, M. (2010). Determination of the degree of N-acetylation for chitin and chitosan by various NMR spectroscopy techniques: A review. *Carbohydrate Polymers, 79*, 801–810.

Lavertu, M., Filion, D., & Buschmann, M. D. (2008). Heat-induced transfer of protons from chitosan to glycerol phosphate produces chitosan precipitation and gelation. *Biomacromolecules, 9*, 640–650.

Li, Y., Toma, R., & Toma, H. (2012). Injectable and biodegradable hydrogels: Gelation, biodegradation and biomedical applications. *Chemical Society Reviews, 41*, 2193–2221.

Mazeau, K., Winter, W. T., & Chanzy, H. (1994). Molecular and crystal structure of a high-temperature polymorph of chitosan from electron diffraction data. *Macromolecules, 27*, 7606–7612.

Meiboom, S., & Gill, D. (1958). Modified SpinEcho method for measuring nuclear relaxation times. *The Review of Scientific Instruments, 29*, 688–691.

Roberts, G. A. F. (1992). *Chitin chemistry*. Houndmills, UK: Macmillan.

Ruel-Gariépy, E., Shive, M., Bichara, A., Berrada, M., Le Garrec, D., Chenite, A., et al. (2004). A thermosensitive chitosan-based hydrogel for the local delivery of paclitaxel. *Euopean Journal of Pharmaceutics and Biopharmaceutics, 57*, 53–63.

Sacco, P., Cok, M., Asaro, F., Paoletti, S., & Donati, I. (2018). The role played by the molecular weight and acetylation degree in modulating the stiffness and elasticity of chitosan gels. *Carbohydrate Polymers, 196*, 405–413.

Schurz, J. (1991). Rheology of polymer solutions of the network type. *Progress in Polymer Science, 16*, 1–53.

Scherer, G. W. (1994). Hydraulic radius and mesh size of gels. *Journal of Sol-Gel Science and Technology, 1*, 285–291.

Singh, N. K., & Lee, D. S. (2014). In situ gelling pH- and temperature-sensitive biodegradable block copolymer hydrogels for drug delivery. *Journal of Controlled Release, 193*, 214–227.

Souza, R. D., Zahedi, P., Allen, C. J., & Piquette-Miller, M. (2009). Biocompatibility of injectable chitosan–phospholipid implant systems. *Biomaterials, 30*, 3813–3824.

Tan, H., Chu, C. R., Payne, K. A., & Marra, K. G. (2009). Injectable in situ forming biodegradable chitosan-hyaluronic acid based hydrogels for cartilage tissue engineering. *Biomaterials, 30*, 2499–2506.

Tømmeraas, K., Vårum, K. M., Christensen, B. E., & Smirsrød, O. (2001). Preparation and characterization of oligosaccharides produced by nitrous acid depolymerization of chitosans. *Carbohydrate Research, 333*, 137–144.

Vårum, K. M., Antohonsen, M. W., Grasdalen, H., & Smidsrød, O. (1991). Determination of the degree of N-acetylation and the distribution of N-acetyl groups in partially N-deacetylated chitins (chitosans) by high-field n.m.r. Spectroscopy. *Carbohydrate Research, 211*, 17–23.

Zhou, H. Y., Jiang, L. J., Cao, P. P., Li, J. B., & Chen, X. G. (2015). Glycerophosphate-based chitosan thermosensitive hydrogels and their biomedical applications. *Carbohydrated Polymers, 117*, 524–536.